Phase Equilibria in the System Hafnia-Yttria-Samaria at 1600 °C

E. Andrievskaya, V. Smirnov and L. Lopato

Institute of Materials Science Problems of Ukrainian National Academy of Sciences, Krzhizhanovsky str. 3, 03142, Kiev, Ukraine

(Received October 30, 2003)

ABSTRACT

The objective of this work is to investigate the phase equilibria in the ternary HfO_2-Y_2O_3-Sm_2O_3 system at 1600 °C and to define the most prospective compositions suitable for the structural and functional ceramics of high ionic conductivity and mechanical strength. The phase compositions of the annealed samples were studied by microstructural, petrographic and X-ray analyses. The experimental isothermal section of the HfO_2-Y_2O_3-Sm_2O_3 system at 1600 °C has been developed. The fields of solid solutions based on M and F-HfO_2, C-Y_2O_3, $Sm_2Hf_2O_7$ (Py), B-Sm_2O_3 were found at 1600 °C.

The isothermal section of the system HfO_2-Y_2O_3-Sm_2O_3 crosses three-phase fields (one - F+B+C; two - F+Py+C) and eight two-phase fields (F+B; C+B; M+F; C+Py; two C+F; two Py+F). Six homogeneity fields based on different polymorphous modifications of initial components have been determined as a sequence of fluorite solubility gap. The upper boundary of fluorite-type ternary solid solutions runs through the composition of 40 mol % HfO_2 - 60 mo l% Sm_2O_3 and maximum yttria solubility corresponds to 38 mol % HfO_2 - 8 mol % Y_2O_3. Therefore, fully stabilized hafnia solid solutions can be found in samaria-rich compositions. In the hafnia-rich field the fluorite solid solutions have maximum extension of 7-55 mol % Y_2O_3 along the binary system HfO_2-Y_2O_3. The upper boundary of this field runs below the isoconcentrate of 80 mol % HfO_2. The refractive indexes of the fluorite-type hafnia and pyrochlore-type compound are around 2,069 and 2,049 respectively.

INTRODUCTION

The HfO_2-Y_2O_3-Sm_2O_3 system is one of the systems with potential technological applications for structural and high-performance functional ceramic materials /1-3/. The phase diagram of this system has not been reported.

The phase equilibria of the boundary binary systems HfO_2-Sm_2O_3, HfO_2-Y_2O_3 and Y_2O_3-Sm_2O_3 are studied quite well at high temperatures /2-17/ The system HfO_2-Y_2O_3 is one with limited mutual solubility of the components in the solid state. It is characterized by the formation of narrow fields of solid solutions based on monoclinic (M-) and tetragonal (T-) HfO_2, an extended field of fluorite-type (F) solid solution and homogeneity fields based on the cubic rare-earth oxide type (C-) and hexagonal rare-earth oxide type (H-) forms of the yttria /2-12/. No compounds were found in the system /9, 11/.

The system HfO_2-Sm_2O_3 is characterized by the fields of solid solutions based on different crystallographic modifications of pure components and intermediate phase $Sm_2Hf_2O_7$ /3, 13-15/. Samarium hafnate is a pyrochlore-type compound, incongruently melted at 2550 ± 25 °C. The lattice parameter for $Sm_2Hf_2O_7$ is equal to 1.0556 nm and refractive index is 2.056. The homogeneity field of the samarium hafnate at 2100 °C is quite wide, 62-69 mol% HfO_2, and the lattice parameter varies from 1.0628 to 1.0506 nm, respectively /15/.

Samaria markedly decreases temperatures of polymorphous transformations in hafnia. The solubility of Sm_2O_3 in monoclinic hafnia is not high (~ 1.5 mol%).

The coordinates of eutectoid corresponding to the transformation M → T HfO_2 are 1750 °C and ~ 98 mol% HfO_2. The solubility of samaria in tetragonal hafnia is also not high (~ 2.5 mol%); however in cubic hafnia, it is much higher, markedly changing with temperature and concentration of Sm_2O_3. The homogeneity field of fluorite solid solutions consists of two parts surrounding a quite wide field of pyrochlore solid solutions. This solubility gap is the main feature of hafnia-REO systems. At 2100 °C the solubility changes from 96 to 77 and from 47.5 to 39 mol% HfO_2. The lattice parameters vary from 0.5156 to 0.5208 and from 0.5358 to 0.5366 nm.

In the system Sm_2O_3-Y_2O_3, the following solid solutions were previously found: B-, A-, H- and X- of Sm_2O_3, as well as C- and H- Y_2O_3 /16, 17/. Temperature of polymorphous transformations in Sm_2O_3 (X ⇄ H; H ⇄ A; A ⇄ B) depends on the content of HfO_2 dissolved. The H- Sm_2O_3 forms continuous row of solid solutions. On the curve, dividing H- and A-, B-, C-fields, there are eutectoid and peritectoid points coordinated as 2050 °C, 30 mol% Y_2O_3 and 2200 °C, 65 mol% Y_2O_3, respectively. The transformation A ⇄ B occurs at higher temperatures then in pure samaria (increases from 1875 to 1925 ± 20 °C). The solubility of Y_2O_3 in B-Sm_2O_3 achieves 40 mol% at 1600 °C. The lattice parameters decrease from a=1.4180, e=0.3636, c=0.8843 nm; β=100.1° to a=1.409, e=0.3556, c=0.875 nm; β=100.1° in saturated solid solutions. The refractive indexes change from n_p=2.10 to n_p=2.038. The C- Y_2O_3 is able to resolve around 50 mol% Sm_2O_3. The lattice parameter increases from a=1.0604 nm in Y_2O_3 to a=1.076 nm in composition 50 mol% Y_2O_3-50 mol% Sm_2O_3. The refraction index varies from n=1.91 to n=1.95 /16/.

EXPERIMENTAL PROCEDURE

Powders of hafnia, yttria and samaria (99.99 %, Doslidnij zavod Phisiko-Khim. Institutu AN Ukrajini, Odesa) were used as raw materials. The set of specimens was prepared from nitrate solutions with their subsequent evaporation and decomposition at 1250°C for 2 h. Powders were pressed into pellets 5 mm in diameter and 5 mm in height. The specimens were prepared in steps of 1, 5 and 10 mol %. To study the phase equilibria, the experimental points locating on the following seven lines were selected: HfO_2 - (50 mol% Y_2O_3-50 mol% Sm_2O_3), Y_2O_3 - (64 mol% HfO_2-36 mol% Sm_2O_3), Y_2O_3 - (50 mol% HfO_2-50 mol% Sm_2O_3), HfO_2 - (15 mol% Y_2O_3 – 85 mol% Sm_2O_3), (55 mol% Y_2O_3 - 45 mol% HfO_2) - (55 mol% Y_2O_3-45 mol% Sm_2O_3), (10 mol% HfO_2 - 90 mol% Sm_2O_3) - (10 mol% HfO_2-90 mol% Y_2O_3), (45 mol% HfO_2-55 mol% Sm_2O_3) - (45 mol% HfO_2-55 mol% Y_2O_3). The experimental points are plotted in Fig. 1. The firing of as-prepared samples was carried out in two stages: at 1250 °C (for 223 h in air) and then at 1600 °C (for10 h in air) in the furnaces with heating elements based on SiC and ZrO_2 respectively.

Stoichiometry of composition was controlled selectively by chemical and X-ray fluorescence spectrum analyses. The boundaries of the phase fields were determined by X-ray (DRON-1.5, Burevestnik, Leningrad), petrographic (MIN-8, optical microscope, LOMO, Leningrad), microstructural phase and electron microprobe X-ray (SUPERPROBE-733, JEOL, Japan, Palo Alto, CA) analysis. Scanning electron microscope (CAMEBAX SX-50, Thompson-CSE, U.K.) was used as well. The refractive indexes were measured in highly refractive immersion media (sulfur-selenium alloys or solutions of arsenic tri-bromide in methylene iodide) with an accuracy of ± 0.02. X-ray diffraction analysis of the samples was performed by a powder method at room temperature (CuKα radiation). The scanning speed of 4 ° 2θ/min was employed in the 80 ° to 15 ° 2θ range. The effective precision of the measurements was ± 0.0002 nm.

RESULTS AND DISCUSSIONS

The isothermal section of the system HfO_2-Y_2O_3-Sm_2O_3 at 1600 °C has been developed (Fig. 1). The initial chemical and phase compositions of the samples, annealed at 1600 °C and the lattice parameters of the equilibrium phases are given in Table. 1. The concentration dependences of lattice parameters are shown in Fig. 2. No ternary compounds were found in the system. There is, however, an incongruently melted

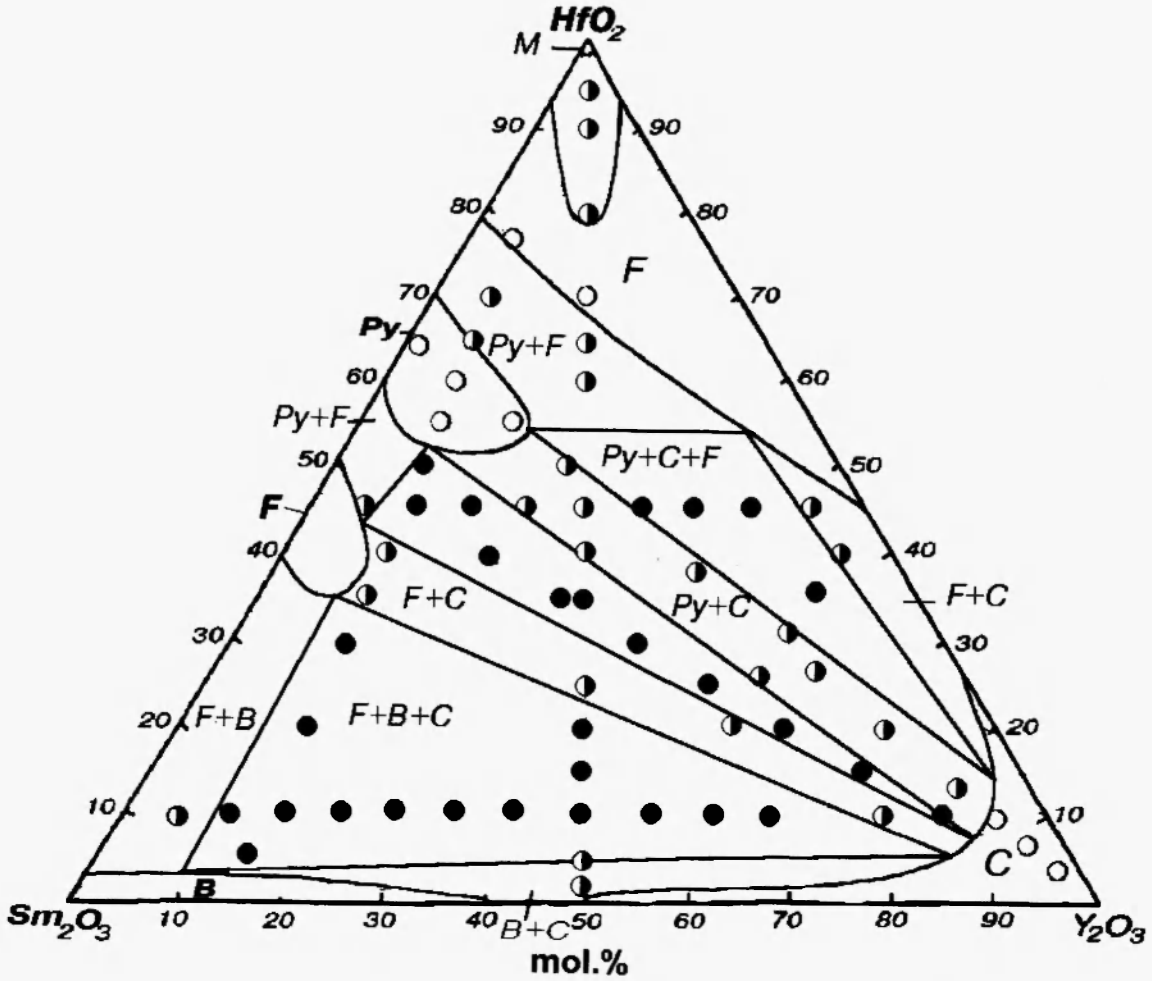

Fig. 1. Isothermal section at 1600 °C for the system HfO_2-Y_2O_3-Sm_2O_3 (○ – single-phase samples, ◑ - binary- phase samples, ● – ternary-phase samples).

binary compound of pyrochlore type in the binary system HfO_2-Sm_2O_3. The compound $Sm_2Hf_2O_7$ is stable in the wide range of temperature and composition (30-40 mol. % Sm_2O_3 at 1600 °C), and therefore the ternary system was triangulated by the section $Sm_2Hf_2O_7$-Y_2O_3. The equilibrium phases based on pyrochlore and C-Y_2O_3 at a given temperature were experimentally revealed in the plane of the section. Therefore, this polythermal section is quasibinary in part and at 1600°C the phase equilibria can be considered separately in the subsystems.

Six homogeneity fields of M- and F-modifications of HfO_2, C-Y_2O_3, B-Sm_2O_3, as well as ordered intermediate samarium hafnate $Sm_2Hf_2O_7$ (Py) were found at 1600 °C. It has been shown that the phase equilibria in the system at a given temperature describe reactions in solid state only.

In the sub-system HfO_2-$Sm_2Hf_2O_7$-Y_2O_3 the boundaries of homogeneity fields change for pyrochlore and fluorite because of solubility. The boundary of solid solution based on monoclinic M-HfO_2 at 1600 °C locates near the composition 99 mol% HfO_2-0.5 mol% Y_2O_3-0.5 mol% Sm_2O_3. This originates from the yttria and samaria solubility in boundary binary systems HfO_2-Sm_2O_3 and HfO_2-Y_2O_3 remaining unchanged in the ternary solutions. The phase field Py is elongated towards the yttria corner and yttria solubility in the pyrochlore achieves 15 mol% Y_2O_3 along the section Y_2O_3 - (64 mol. HfO_2 % - 36 mol% Sm_2O_3). The refractory index of the pyrochlore phase decreases from

Table 1

Chemical and phase compositions of some samples in the HfO_2-Y_2O_3-Sm_2O_3 system heat-treated at 1600 °C (XRD and petrography data)

Composition, mol%		Phase composition by XRD data	Phase composition and refractive indexes by petrography
HfO_2	Y_2O_3		
1	2	3	4
		Section Y_2O_3 - (64 mol% HfO_2 - 36 mol% Sm_2O_3)	
64	0	Py	Py, $n_{(Py)}$=2.056
62	2	Py	Py, $n_{(Py)} \sim 2.056$
62	3	Py	Py, $n_{(Py)} \geq 2.042$
60	5	Py	Py, $n_{(Py)} = 2.042$
57	10	Py	Py, $n_{(Py)} \sim 2.02$
51	20	Py+C	Py+<C>, $n_{(Py)} \geq 2.02$
44	30	Py+C	Py+<C>, $n_{(Py)} = 2.02$; $1.95 < n_{(C)} < 1.98$
38	40	Py+C	Py+<C>, $n_{(Py)} \geq 1.99$; $n_{(C)} \sim 1.96$
32	50	Py+C	Py+<C>, $n_{(Py)} \sim 1.99$; $1.94 < n_{(C)} < 1.95$
29	55	Py+C	Py+<C>, $n_{(Py)} = 1.98$; $n_{(C)} = 1.93$
25	60	Py+C	Py+<C>, $n_{(Py)} = 1.98$; $n_{(C)} < 1.93$
22	65	Py+C	Py+<C>
19	70	Py+C	Py+<C>, $n_{(Py)} = 1.98$; $n_{(C)} \geq 1.92$
16	75	Py+C	Py+<C>, $n_{(Py)} \sim 1.98$; $n_{(C)} > 1.92$
13	80	Py+C	Py+<C>осн., $n_{(Py)} \sim 1.98$; $n_{(C)} > 1.92$
10	85	C	<C>, $1.91 < n_{(C)} < 1.92$
7	90	C	<C>, $1.91 < n_{(C)} < 1.92$
3	95	C	<C>, $n_{(C)} > 1.91$
		Isoconcentrate 45 mol% HfO_2	
45	5	F+Py	<F>+Py, $n_{(Py)} \sim 2.02$
45	10	F+Py+C	<F>+Py+<C>
45	15	F+Py+C	<F>+Py+<C>, $n_{(Py)} > 2.00$; $n_{(F)} < 2.02$
45	20	Py+C	Py+<C>, $n_{(Py)} > 2.00$
45	25	Py+C	Py+<C>, $n_{(Py)} > 2.00$; $n_{(C)} \sim 1.939$
45	30	F+Py+C	<F>+Py+<C>, $n_{(C)} \sim 1.939$
45	35	F+Py+C	<F>+Py+<C> $n_{(C)} \geq 1.939$; $n_{(Py)} \sim 2.00$; $n_{(F)} \sim 1.99$
45	40	F+Py+C	<F>+Py+<C> $n_{(C)} \sim 1.939$; $n_{(Py)} \sim 2.00$; $n_{(F)} \sim 1.96$-1.98
45	45	F+Py+C	<F>+Py+<C> $n_{(C)} \sim 1.94$; $n_{(F)} \sim 1.96$-1.98
45	50	F+C	<F>+<C> $n_{(C)} \geq 1.92$; $n_{(F)} \sim 1.96$-1.98
		Section HfO_2 - (15 mol% Y_2O_3 - 85 mol% Sm_2O_3)	
75	4	F	<F>, $n_{(F)} \sim 2.069$
70	5	F+Py	Py+<F>, $n_{(Py)} \geq 2.069$; $n_{(F)} \leq 2.069$
65	6	F+Py	Py+<F>, $n_{(Py)} \geq 2.069$; $n_{(F)} \sim 2.042$

Table 1 (continued)

1	2	3	4
60	6	Py	Py, $n_{(Py)} > 2.042$
55	7	Py	$n_{(Py)} \leq 2.032$
50	8	F+Py+C	<F>+Py+<C> $n_{(C)} \sim 1.93$; $n_{(Py)} \sim 2.032$; $n_{(F)} \sim 2.02$
45	8	F+Py+C	<F>+Py+<C> $n_{(C)} \sim 1.939$; $n_{(Py)} \sim 2.02$; $n_{(F)} > 2.00$
40	10	F+C	<F>+<C> $n_{(C)} \geq 1.939$; $n_{(F)} \sim 2.00$
35	10	F+C	<F>+<C> $n_{(C)} \geq 1.939$; $1.98 \leq n_{(F)} \geq 1.98$
30	10	B+C+F	<B>+<C>+<F> $n_{(C)} \geq 1.939$; $1.98 \leq n_{(F)} \geq 1.98$
20	12	B+C+F	<B>+<C>+<F> $n_{p(B)} < 2.069$, $n_{g(B)} > 2.069$; $n_{(F)} \sim 2.00$-1.99
10	14	B+C+F	<B>+<C>+<F> $n_{p(B)} < 2.069$, $n_{g(B)} > 2.069$; $n_{(F)} \sim 1.978$; $n_{(C)} \sim 1.931$
5	15	B+C+F	<B>+<C>+<F> $n_{p(B)} < 2.069$, $n_{g(B)} > 2.069$; $n_{(F)} \sim 1.978$; $n_{(C)} < 1.93$
		Isoconcentrate 55 mol% Y_2O_3	
40	55	F+C	<F>+<C>, $n_{(F)} > 1.960$; $n_{(C)} \sim 1.92$
35	55	Py+C+F	Py+<C>+<F>, $n_{(F)} \geq 1.969$; $n_{(C)} \sim 1.92$
30	55	Py+C	Py+<C>, $n_{(Py)} \sim 2.00$; $n_{(C)} \sim 1.931$
25	55	Py+C	Py+<C>, $n_{(Py)} \sim 2.00$; $n_{(C)} \sim 1.931$
20	55	F+C	<F>+<C>
15	55	F+B+C	<F>+<B>+<C>
10	55	F+B+C	<F>+<B>+<C>
5	55	B+C	<B>+<C
		Isoconcentrate 10 mol% HfO_2	
10	5	F+B	<F> + <B>, $n_{(F)} \sim 2.01$; $n_{(B)} > 2.06$
10	10	F+B+C	<F> + <B> + <C>, $n_{(F)} \sim 2.00$; $n_{(B)} \sim 2.06$; $n_{(C)} \sim 1.93$
10	20	F+B+C	<F> + <B> + <C>, $n_{(F)} \sim 2.00$; $n_{(B)} \sim 2.06$; $n_{(C)} \sim 1.93$
10	25	F+B+C	<F> + <B> + <C>, $n_{(F)} \sim 1.96$; $n_{(B)} \sim 2.06$; $n_{(C)} = 1.93$
10	30	F+B+C	<F> + <B> + <C>, $n_{(F)} \sim 1.95$; $n_{(B)} \sim 2.06$; $n_{(C)} \sim 1.93$
10	35	F+B+C	<F> + <B> + <C>, $n_{(F)} \sim 1.95$; $n_{(B)} \sim 2.06$; $n_{(C)} \sim 1.94$
10	40	F+B+C	<F> + <B> + <C>, $n_{(F)} \geq 1.95$; $n_{(B)} \sim 2.06$; $n_{(C)} \sim 1.94$

Table 1 (continued)

1	2	3	4
10	50	F+B+C	<F> + <B> + <C>, $n_{(F)} \sim 1.95$; $n_{(B)} \sim 2.06$; $n_{(C)} \sim 1.93$
10	60	F+B+C	<F> + <B> + <C>, $n_{(F)} \sim 1.95$; $n_{(B)} \sim 2.06$; $n_{(C)} \leq 1.93$
		Section HfO_2-(50 mol% Y_2O_3-50 mol% Sm_2O_3)	
98	1	M+F	<M>+<F>, $n_{(M)} > 2.07$; $n_{(F)} \sim 2.07$
95	2.5	M+F	<M>+<F>, $n_{(M)} > 2.07$; $n_{(F)} \sim 2.07$
90	5	M+F	<M>+<F>, $n_{(M)} > 2.07$; $n_{(F)} > 2.07$
80	10	M+F	<M>+<F>, $n_{(M)} > 2.07$; $n_{(F)} > 2.07$
70	15	F	<F>
65	17.5	Py+F	<F>+Py, $n_{(F)} \sim 2.03$; $n_{(Py)} \sim 2.05$
60	20	Py+F	<F>+Py, $n_{(F)} \sim 2.02$; $n_{(Py)} > 2.02$
55	22.5	Py+F	<F>+Py
50	25	Py+C+F	Py+<C>+<F>
45	27.5	Py+C	<C>+Py, $n_{(C)} \sim 1.94$; $n_{(Py)} \sim 2.02$
40	30	Py+C	Py+<C>
35	32.5	C+F+Py	<C>+<F>+Py, $n_{(C)} \sim 1.93$; $n_{(F)} \sim 1.96$
30	35	F+C	<F>+<C>
25	37.5	F+C	<F>+<C>, $n_{(C)} \sim 1.92$; $1.94 < n_{(F)} < 1.95$
20	40	F+B+C	<F>+<B>+<C>
15	42.5	F+B+C	<F>+<B>+<C>
10	45	F+B+C	<F>+<B>+<C>, $n_{(F)} \geq 1.94$; $n_{(C)} > 1.92$
5	47.5	C+B	<C>+<B>
3	48.5	C+B	<C>+<B>
		Section Y_2O_3-(50 mol% HfO_2-50 mol% Sm_2O_3)	
47	5	F+Py	<F>+Py, $n_{(F)} \sim 1.939$; $n_{(Py)} \sim 2.02$
42	15	F+Py+C	<F>+Py+<C>, $n_{(F)} \sim 1.939$; $n_{(Py)} \sim 2.00$
40	20	F+Py+C	<F>+Py+<C>, $n_{(F)} \sim 1.939$; $n_{(Py)} \sim 2.00$
37	25	F+Py+C	<F>+Py+<C>
35	30	F+Py+C	<F>+Py+<C>, $n_{(F)} \sim 1.939$; $n_{(Py)} > 1.96$
30	40	F+Py+C	<F>+Py+<C> $n_{(F)} > 1.93$; $n_{(Py)} \sim 2.02$; $n_{(C)} \sim 1.93$
27	45	F+Py+C	<F>+Py+<C> $n_{(F)} > 1.93$; $n_{(Py)} \sim 2.02$; $n_{(C)} \sim 1.93$
25	50	F+Py+C	<F>+Py+<C> $n_{(F)} > 1.93$; $n_{(Py)} \sim 2.01$; $n_{(C)} \sim 1.93$
20	60	F+Py+C	<F>+Py+<C> $n_{(F)} > 1.93$; $n_{(Py)} \sim 2.02$; $n_{(C)} \sim 1.92$
18	65	F+Py+Cосн.	<F>+Py+<C> $n_{(F)} > 1.93$; $n_{(Py)} \sim 2.01$; $n_{(C)} \sim 1.92$
15	70	F+Py+C	<F>+Py+<C> $n_{(F)} > 1.93$; $n_{(Py)} \sim 2.00$; $n_{(C)} \sim 1.92$
12	75	F+Py+C	<F>+Py+<C>осн. $n_{(F)} > 1.93$; $n_{(Py)} \sim 2.00$; $n_{(C)} \sim 1.91$

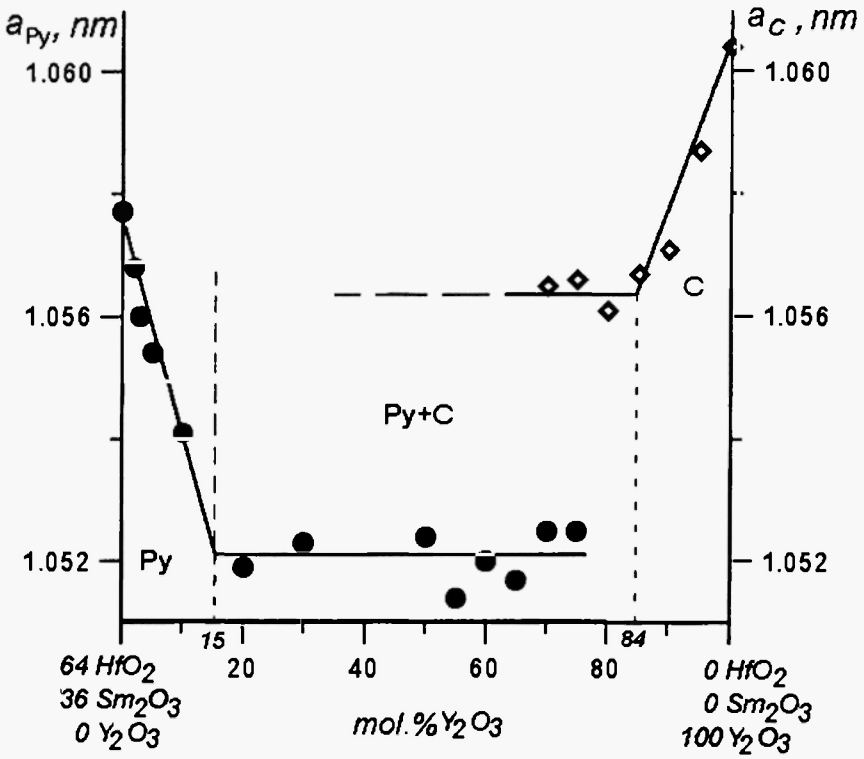

Fig. 2. Concentration dependences of lattice parameters for solid solutions based on C-Y_2O_3 (◇) and pyrochlore intermediate phase $Sm_2Hf_2O_7$ (Py) (•) along the Y_2O_3 - (64 mol% HfO_2-36 mol% Sm_2O_3) section in the system HfO_2-Y_2O_3-Sm_2O_3 heat-treated at 1600 °C.

n=2.056 in pure phase to n=2.02 in saturated solid solution. A specific microstructure inherent in pyrochlore solid solution 57 mol% HfO_2-10 mol% Y_2O_3- 33 mol% Sm_2O_3 is presented by coarse and small (1.3-44.4 μm) grains with intragrained porosity (Fig. 3a). The electron microprobe X-ray spectral analysis showed that the sample is single phase and all the elements (Hf, Y, Sm) were uniformly distributed through the sample. This observation correlates with XRD and petrography data (see Table 2) and confirms formation of solid solution based on ordered $Sm_2Hf_2O_7$ (Py).

Samples of the following compositions: 51 mol% HfO_2-20 mol% Y_2O_3-29 mol% Sm_2O_3, 44 mol% HfO_2-30 mol% Y_2O_3-26 mol% Sm_2O_3, 32 mol% HfO_2-50 mol% Y_2O_3-18 mol% Sm_2O_3, 13 mol% HfO_2-80 mol% Y_2O_3-7 mol% Sm_2O_3, 30 mol% HfO_2-55 mol% Y_2O_3-15 mol% Sm_2O_3, 25 mol% HfO_2-55 mol% Y_2O_3-20 mol% Sm_2O_3 and 45 mol% HfO_2-27.5 mol% Y_2O_3-27.5 mol% Sm_2O_3 define the boundary of the two phase field (Py+C). The microstructure of the last composition is presented in Fig. 3b. Two clearly seen structural components can be distinguished by contrast. By the data of qualitative local x-ray analysis (Fig. 4 a-e) one can conclude that the dark phase is enriched with yttria, contains less hafnia and samaria and corresponds to solid solution based on Y_2O_3. The light-colored phase is $Sm_2Hf_2O_7$, because it contains more heavy elements such as samarium and hafnium compared to dark colored phase.

The maximal solubility of the pyrochlore phase in the C-Y_2O_3 solid solution at 1600 °C along the section Py-Y_2O_3 corresponds to the composition 10 mol% HfO_2-85 mol% Y_2O_3-5 mol% Sm_2O_3. The refractive index varies from n=1.91 in pure Y_2O_3 to n=1.96 in saturated solid solution <C-Y_2O_3>.

In the subsystem HfO_2-$Sm_2Hf_2O_7$-Y_2O_3, the fluorite solid solution F-HfO_2 showed the maximum of solubility but the total solubility of dopants in hafnia is markedly decreased while increasing content of the

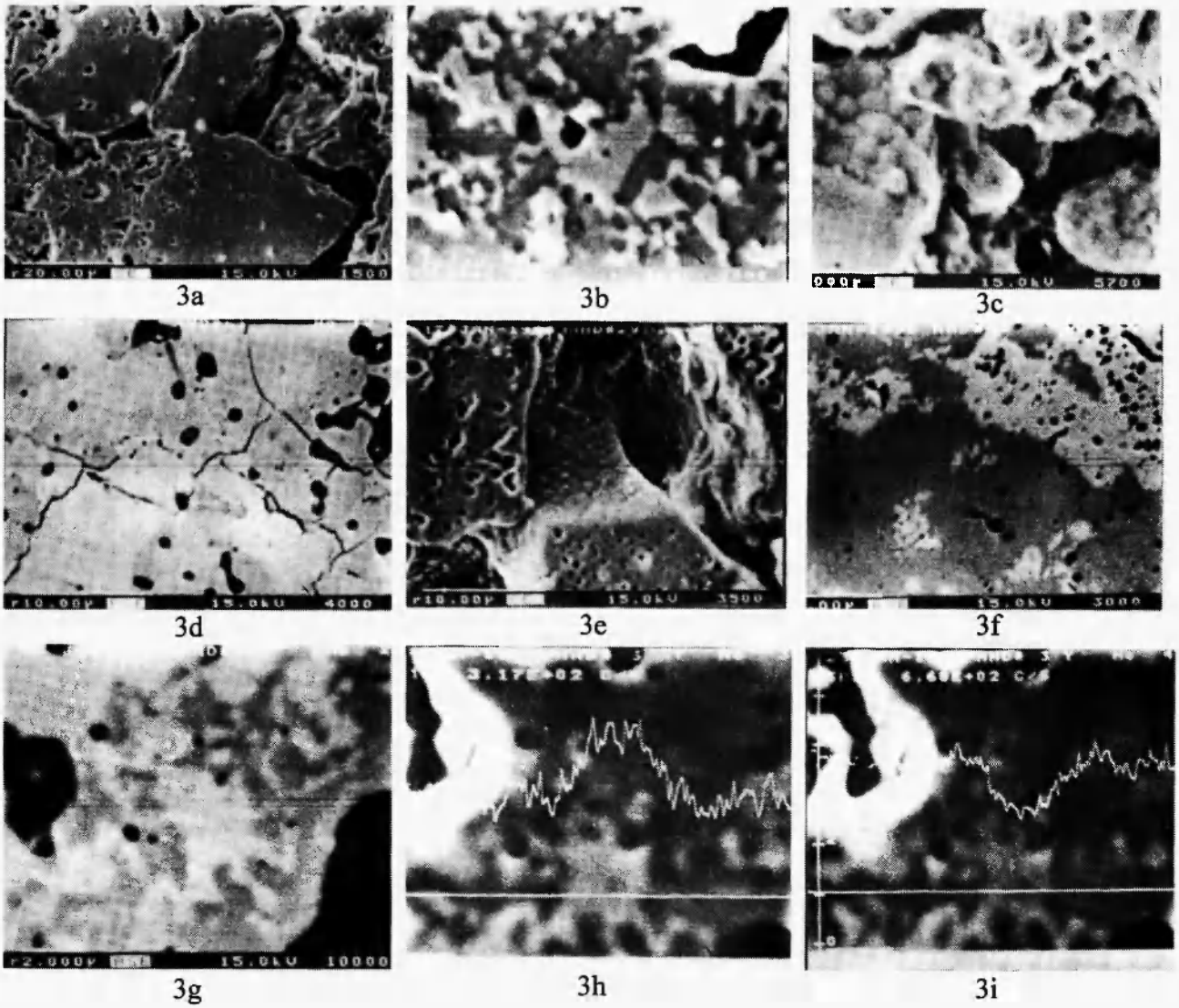

Fig. 3. Microstructures of the samples and element distribution through the samples in the definite field of compositions of the sub-system HfO_2-$Sm_2Hf_2O_7$-Y_2O_3 heat-treated at 1600 °C: **(a)** Py, 57 mol% HfO_2-10 mol% Y_2O_3-33 mol% Sm_2O_3; **(b)** Py+<C>, light is Py, gray is <C>, black is pore, 32 mol% HfO_2-50 mol% Y_2O_3-18 mol% Sm_2O_3; **(c)** Py+<F>, light is <F-HfO_2>, gray is Py, black is pore, 70 mol% HfO_2-5 mol% Y_2O_3-25 mol% Sm_2O_3; **(d)** <M>+<F>, light is <M-HfO_2>, gray is <F-HfO_2>, black is pore, 95 mol% HfO_2-2.5 mol% Y_2O_3-2.5 mol% Sm_2O_3; **(e)** <C>+<F>, light coarse grains are <F-HfO_2>, gray is <C-Y_2O_3>, 45 mol% HfO_2-50 mol% Y_2O_3-5 mol% Sm_2O_3; **(f)** <C>+<F>, light is <F-HfO_2>, gray is <C-Y_2O_3>, black is pore,40 mol% HfO_2-55 mol% Y_2O_3-5 mol% Sm_2O_3; **(g)** <C>+<F>, light is <F-HfO_2>, gray is <C-Y_2O_3>, black is pore, 40 mol% HfO_2-55 mol% Y_2O_3-5 mol% Sm_2O_3; **(h)** <F>+<C>, Hf, light is <F-HfO_2>, gray is <C-Y_2O_3>, black is pore, 40 mol% HfO_2-55 mol% Y_2O_3-5 mol% Sm_2O_3; **(i)** <F>+<C>, Y, light is <F-HfO_2>, gray is <C-Y_2O_3>, black is pore, 40 mol% HfO_2-55 mol% Y_2O_3-5 mol% Sm_2O_3.

Table 2
The coordinates of the tie-line triangle in the system HfO_2-Y_2O_3-Sm_2O_3 at 1600 °C

Phase Field	Coordinates of the tie-line triangle, mol%									
	F		Py		F		C		B	
	HfO_2	Y_2O_3	HfO_2	Y_2O_3	HfO_2	Y_2O_3	HfO_2	Y_2O_3	HfO_2	Y_2O_3
Py+F+C	54.0	39.0	54.0	15.0	-	-	15.0	82.0	-	-
Py+F+C	-	-	53.0	8.0	43.0	6.0	8.0	84.0	-	-
F+B+C	-	-	-	-	36.0	7.0	7.0	83.0	3.0	9.0

third component (samaria): in the boundary binary system HfO_2-Y_2O_3 the solubility changes in the range 45-93 mol% HfO_2 but the upper boundary of the homogeneity field goes below an isoconcentrate line 80 mol% HfO_2 and the sample 75 mol% HfO_2-12.5 mol% Y_2O_3-12.5 mol% Sm_2O_3 is still single phase (F). The sample 80 mol% HfO_2-10 mol% Y_2O_3-10 mol% Sm_2O_3 is two phase (M+F). The low limit of solubility corresponds to the boundary passing through the following compositions 75 mol% HfO_2-4 mol% Y_2O_3-21 mol% Sm_2O_3 and 65 mol% HfO_2-17.5 mol% Y_2O_3-17.5 mol% Sm_2O_3. The refractory index of the fluorite type cubic phase is of n = 2.069. The sample containing 70 mol% HfO_2-5 mol% Y_2O_3-25 mol% Sm_2O_3 is two phase (F+Py), though x-ray peaks of samarium hafnate is rather weak. XRD data are confirmed by petrography

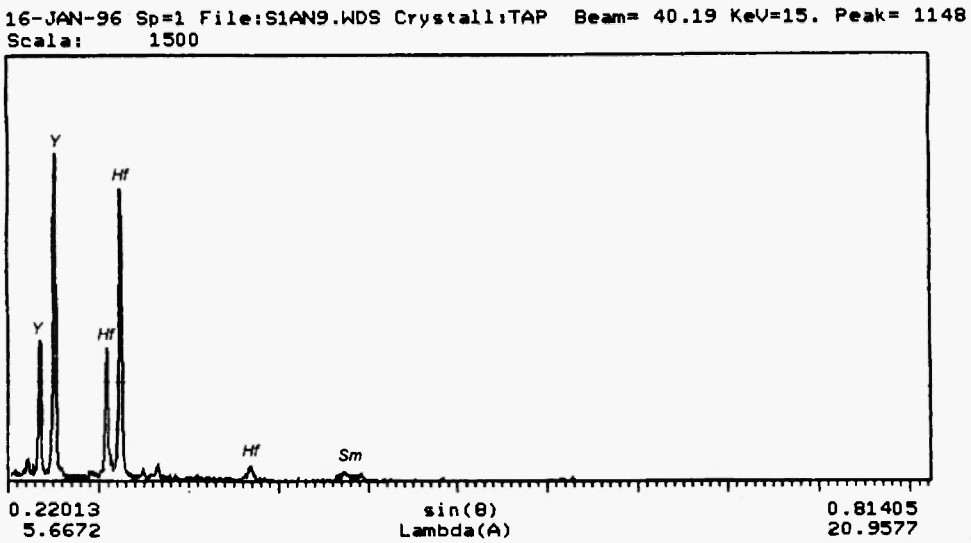

(a)

Fig. 4. Element distribution in definite phase field of the sub-system HfO_2-$Sm_2Hf_2O_7$-Y_2O_3 heat-treated at 1600 °C: **(a)** 32 mol% HfO_2-50 mol% Y_2O_3-18 mol% Sm_2O_3, Py+C, Sp.= 1, elements: Y; Hf, scale = 1500, light phase; **(b)** 32 mol% HfO_2-50 mol% Y_2O_3-18 mol% Sm_2O_3, Py+C, Sp.= 1, elements: Y; Hf, scale = 1553, gray phase; **(c)** 32 mol% HfO_2-50 mol% Y_2O_3-18 mol% Sm_2O_3, Py+C, Sp.= 1, elements:Y; Hf, scale = 1600, light and gray phase; **(d)** 32 mol% HfO_2-50 mol% Y_2O_3-18 mol% Sm_2O_3, Py+C, Sp.= 2, scale = 150, light and gray phase; **(e)** 32 mol% HfO_2-50 mol% Y_2O_3-18 mol% Sm_2O_3, Py+C, Sp.= 3, elements: Sm,Y, scale = 400; light and gray phase; **(f)** 40 mol% HfO_2-55 mol% Y_2O_3-5 mol% Sm_2O_3, F+C, Sp.= 1, elements: Y; Hf, scale = 500, light phase; **(g)** 40 mol% HfO_2-55 mol% Y_2O_3-5 mol% Sm_2O_3, F+C, Sp.= 1, elements: Y; Hf, scale = 500, Sp.= 1, elements: Y; Hf, gray phase.

continued...

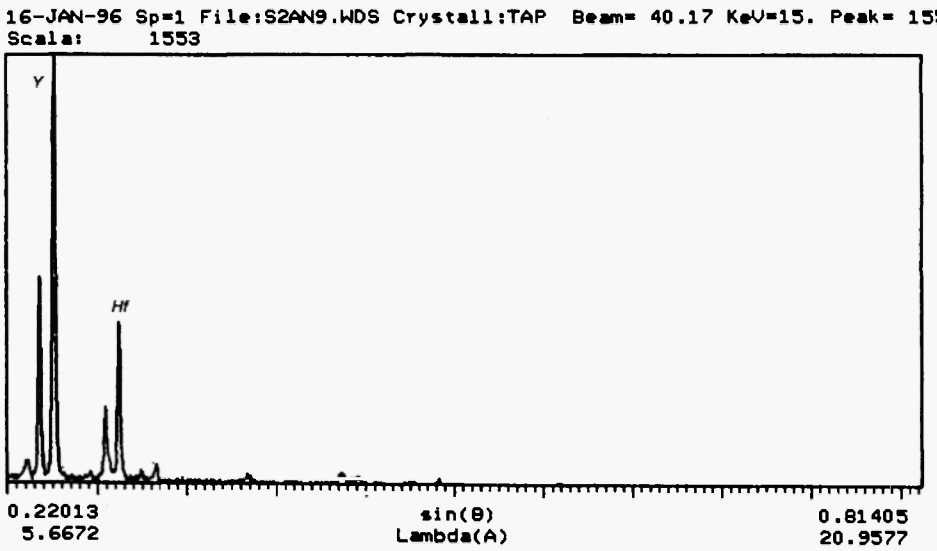

(b)

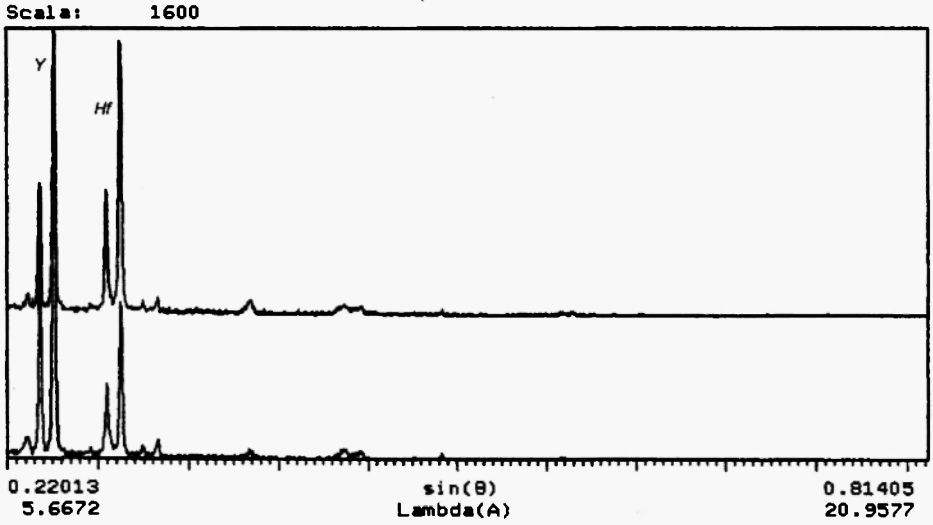

(c)

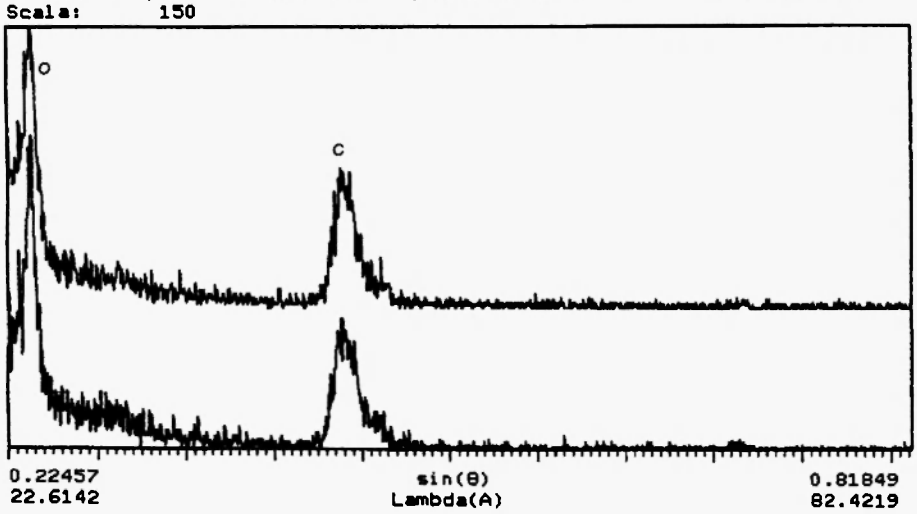

(d)

continued...

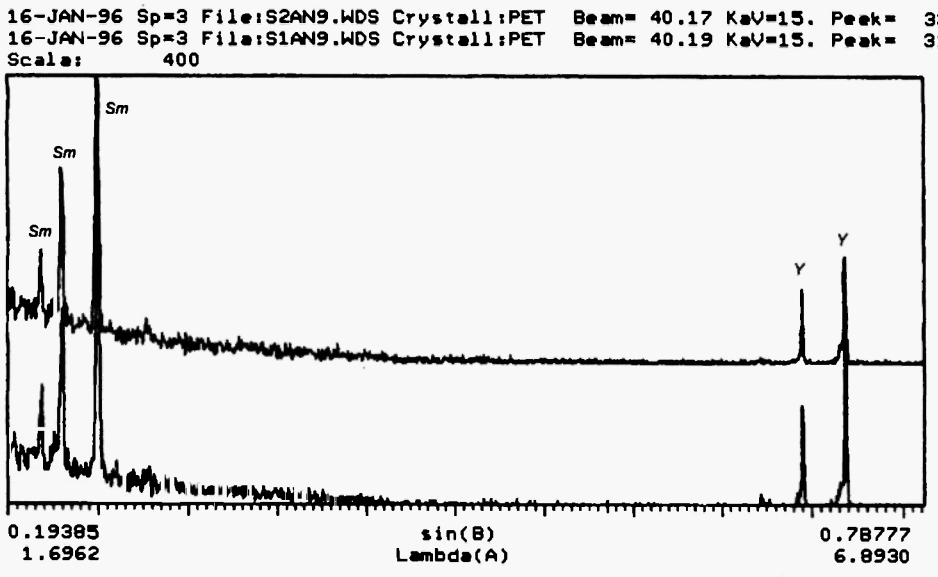
16-JAN-96 Sp=3 File:S2AN9.WDS Crystall:PET Beam= 40.17 KeV=15. Peek= 332
16-JAN-96 Sp=3 File:S1AN9.WDS Crystall:PET Beam= 40.19 KeV=15. Peak= 319
Scala: 400
Sm
Sm
Sm
Y
Y
0.19385
1.6962
sin(B)
Lambda(A)
0.78777
6.8930

(e)

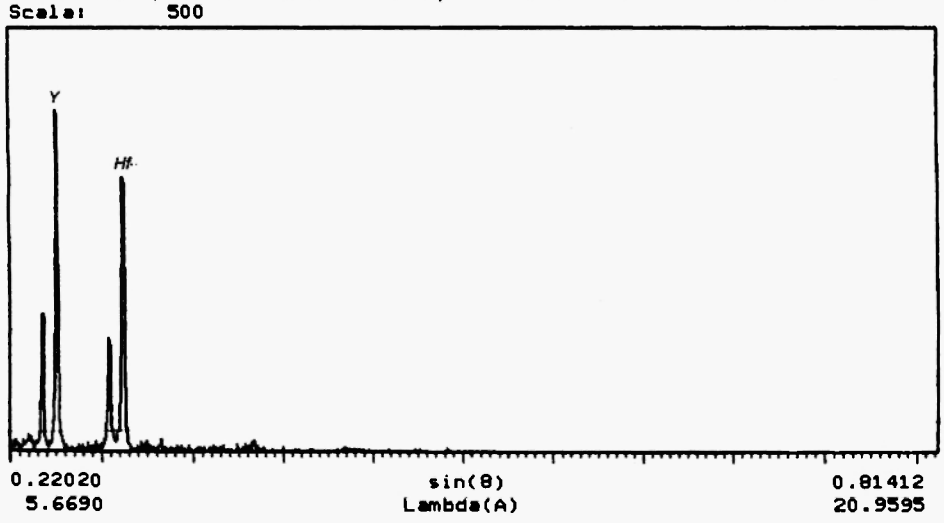
22-JAN-96 Sp=1 File:S1AN43.WDS Crystall:TAP Beam= 9.95 KeV=15. Peak= 402
Scala: 500
Y
Hf
0.22020
5.6690
sin(B)
Lambda(A)
0.81412
20.9595

(f)

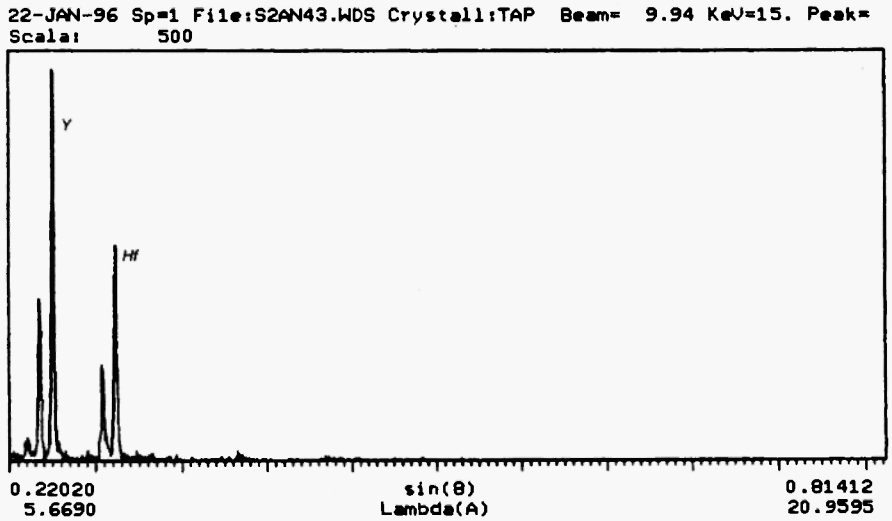
22-JAN-96 Sp=1 File:S2AN43.WDS Crystall:TAP Beam= 9.94 KeV=15. Peak= 478
Scala: 500
Y
Hf
0.22020
5.6690
sin(B)
Lambda(A)
0.81412
20.9595

(g)

data and the two isotropic phases are distinguished by the refractory indexes of n= 2.069 (F) and n=2.049 (Py).

The fluorite type phase exists in the two phase (F+Py; F+C; F+M) and three phase (F+B+C; F+Py+C) fields.

There is one three phase field (Py+F+C) in the isothermal section of the subsystem HfO_2-$Sm_2Hf_2O_7$-Y_2O_3 at 1600° C. The boundaries of the phase fields wee determined from x-ray phase analysis of the following compositions: 65 mol% HfO_2-6 mol% Y_2O_3-29 mol% Sm_2O_3, 60 mol% HfO_2-20 mol% Y_2O_3-20 mol% Sm_2O_3 are two phase (Py+F); 45 mol% HfO_2-30 mol% Y_2O_3-25 mol% Sm_2O_3, 45 mol% HfO_2-35 mol% Y_2O_3-20 mol% Sm_2O_3, 45 mol% HfO_2-40 mol% Y_2O_3-15 mol% Sm_2O_3, 45 mol% HfO_2-45 mol% Y_2O_3-10 mol% Sm_2O_3 are three phase (Py+F+C); 45 mol% HfO_2-50 mol% Y_2O_3-5 mol% Sm_2O_3, 40 mol% HfO_2-55 mol% Y_2O_3-5 mol% Sm_2O_3 are two phase (F+C). XRD data correlate with petrography and electron microscopy including samples of boundary compositions (Table 1).

The boundary dividing the homogeneity fields of $Sm_2Hf_2O_7$ and F-HfO_2 at 1600 °C is drawn as a result of phase analysis in the samples 65 mol% HfO_2-6 mol% Y_2O_3-29 mol% Sm_2O_3, by both XRD and petrography (Table 1). The microstructure of the two phase field (Py+F) is shown in Fig. 3c. The sample 70 mol% HfO_2-5 mol% Y_2O_3-25 mol% Sm_2O_3 has two structural components. According to the SEM analysis, the microstructure is represented by matrix phase with polyhedral-shaped grains with size of 5.5-6.6 μm and second phase locating on grain boundaries with irregular-shaped fine grains of 1.1-2.2 μm. In accordance with the results of XRD and petrography, this sample is two phase composition (Py+F). The local x-ray spectral analysis confirmed this conclusion and the intergraine phase was enriched with hafnia and indicated as F-HfO_2. The matrix phase was enriched with samaria and hafnia, which means that the pyrochlore $Sm_2Hf_2O_7$ (Py) was identified. The quantity of F- phase increases with concentration of hafnia.

Using XRD data and electron microscopy, the coordinates of tie-line triangle were determined for three phase field (Py+F+C) (Table 2).

The microstructure of the sample 95 mol% HfO_2-2.5 mol% Y_2O_3-2.5 mol% Sm_2O_3, is two phase and according to XRD corresponds to the field (M+F). Both phases are clearly seen in Fig. 3d. The distribution of the main elements through the sample is not uniform: both phases contain hafnia but different proportions of yttria and samaria in different grains, higher content in dark grains, which are F-solid solutions. The light phase contains a few yttria and samaria and represents M-HfO_2.

The samples 45 mol% HfO_2-30 mol% Y_2O_3-25 mol% Sm_2O_3, 45 mol% HfO_2-35 mol% Y_2O_3-20 mol% Sm_2O_3, 45 mol% HfO_2-40 mol% Y_2O_3-15 mol% Sm_2O_3 and 45 mol% HfO_2-45 mol% Y_2O_3-10 mol% Sm_2O_3 determine the boundary of three phase field (Py+F+C).

The microstructures and concentration profiles characterizing the two phase field (F+C) in the subsystem HfO_2-$Sm_2Hf_2O_7$-Y_2O_3 are represented in Figs. 3 e-i and 4. f, g. The two structural components differ by contrast. One can conclude that the dark phase is enriched with yttria, contains less hafnia, samaria and corresponds to solid solution based on Y_2O_3. The light phase corresponds to F-HfO_2.

The isothermal section of the sub-system Sm_2O_3-$Sm_2Hf_2O_7$-Y_2O_3 at 1600 °C crosses two three phase (Py+F+C, F+B+C) and five two phase fields (Py+F, F+B, Py+C, F+C, B+C). The microstructures and concentration profiles of some samples possessing different phase fields are shown in Fig. 5. In the subsystem with low content of HfO_2 the following solid solutions based on F-HfO_2, B-Sm_2O_3, C-Y_2O_3 and intermediate phase Py were revealed.

As soon as the field of solid solutions based on cubic HfO_2 in the binary system HfO_2-Sm_2O_3 expires gap and two homogeneity fields of the fluorite phase were expected. In accordance with experimental results, the boundary of solid solutions of F-HfO_2 in this sub-system varies from 40 and 50 mol% HfO_2 in binary system toward to the yttria comer. The maximum solubility of yttria in the fluorite solid solution corresponds to the composition 38 mol% HfO_2- 8 mol% Y_2O_3- 54 mol% Sm_2O_3.

The homogeneity field of B-Sm_2O_3 phase is quite wide (up to 40 mol% Y_2O_3). The solubility of HfO_2 in the B- Sm_2O_3 is negligible, and does not exceed ~ 3 mol% HfO_2.

The boundaries of the two phase fields (B+C) in the ternary system become wider. The sample 5 mol% HfO_2-55 mol% Y_2O_3-40 mol% Sm_2O_3 was studied in details. By the data of scanning electron microscopy the

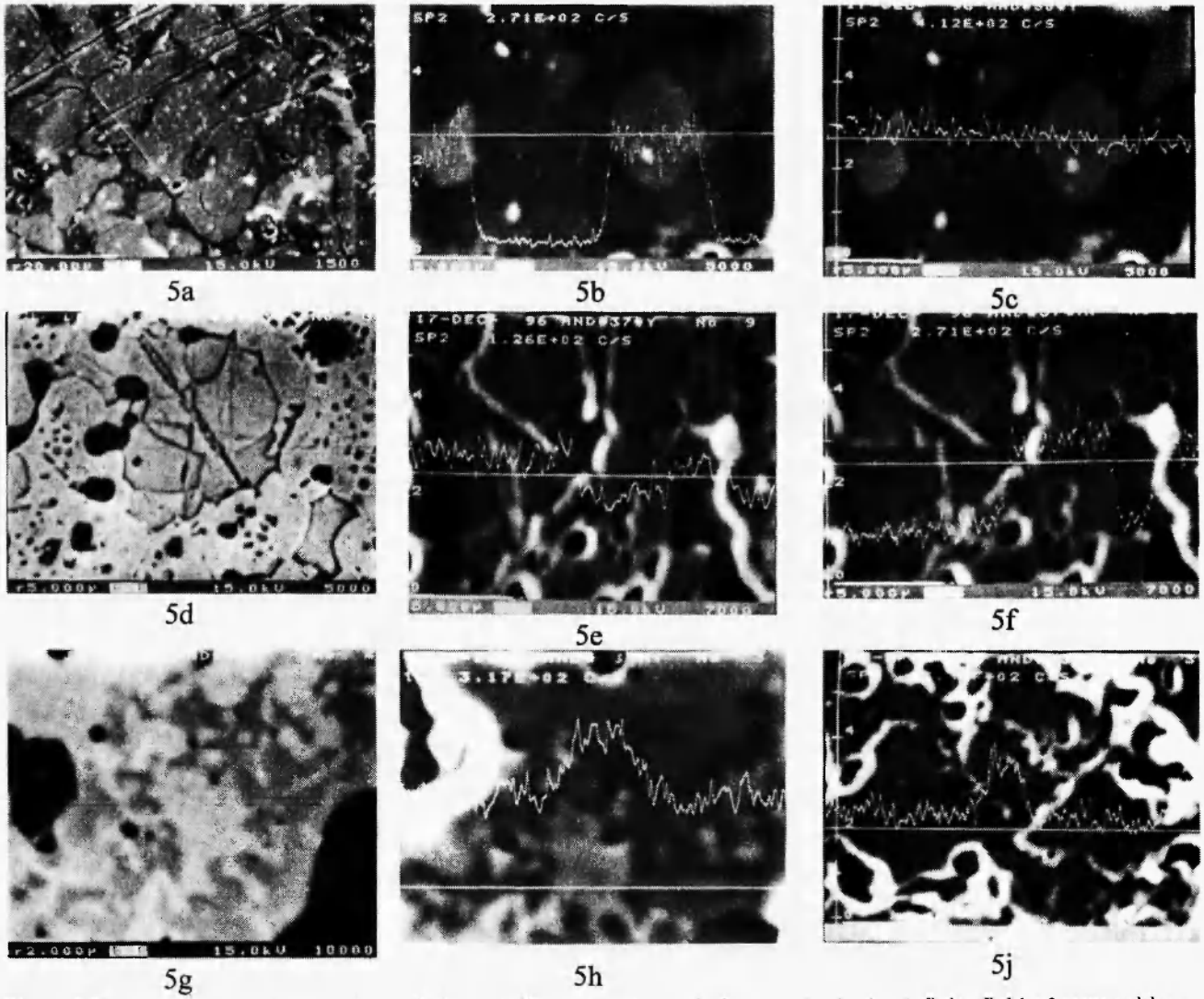

Fig. 5. Microstructures of the samples and element distribution through the samples in the definite field of compositions of the sub-system Sm_2O_3- $Sm_2Hf_2O_7$-Y_2O_3 heat-treated at 1600 °C: **(a)** <B>+<C>, light is <C-Y_2O_3>, gray is <B-Sm_2O_3>, black is pore, 5 mol% HfO_2-55 mol% Y_2O_3-40 mol% Sm_2O_3; **(b)** <B>+<C>, Hf, 5 mol% HfO_2-55 mol% Y_2O_3-40 mol% Sm_2O_3; **(c)** <B>+<C>, Y, 5 mol% HfO_2-55 mol% Y_2O_3-40 mol% Sm_2O_3; **(d)** <F>+<C>, light is <F-HfO_2>, dark is <C-Y_2O_3>, 40 mol% HfO_2-10 mol% Y_2O_3-50 mol% Sm_2O_3; **(e)** <F>+<C>, Y, 40 mol% HfO_2-10 mol% Y_2O_3-50 mol% Sm_2O_3; **(f)** <F>+<C>, Hf, 40 mol% HfO_2-10 mol% Y_2O_3-50 mol% Sm_2O_3; **(g)** <F>+<C>, light is <F-HfO_2>, dark matrix is <C-Y_2O_3>, 30 mol% HfO_2-35 mol% Y_2O_3-35 mol% Sm_2O_3; **(h)** <F>+<C>, 25 mol% HfO_2-37.5 mol% Y_2O_3-37.5 mol% Sm_2O_3; **(i)** <F>+<C>, Y, 25 mol% HfO_2-37.5 mol% Y_2O_3-37.5 mol% Sm_2O_3; **(j)** <F>+<C>, Hf, 25 mol% HfO_2-37.5 mol% Y_2O_3-37.5 mol% Sm_2O_3; **(k)** <B>+<C>+<F>, light is <F>, gray is <C-Y_2O_3>, dark is <B-Sm_2O_3>, 30 mol% HfO_2-10 mol% Y_2O_3-60 mol% Sm_2O_3; **(l)** <B>+<C>+<F>, Hf, 30 mol% HfO_2-10 mol% Y_2O_3-60 mol% Sm_2O_3; **(m)** <B>+<C>+<F>, Y, 30 mol% HfO_2-10 mol% Y_2O_3-60 mol% Sm_2O_3; **(n)** <B>+<C>+<F>, 20 mol% HfO_2-12 mol% Y_2O_3-68 mol% Sm_2O_3; **(o)** <B>+<C>+<F>, Hf, 20 mol% HfO_2-12 mol% Y_2O_3-68 mol% Sm_2O_3; **(p)** <B>+<C>+<F>, Y, 20 mol% HfO_2-12 mol% Y_2O_3-68 mol% Sm_2O_3; **(q)** <B>+<C>+<F>, light is <F>, gray is <C-Y_2O_3>, dark is <B-Sm_2O_3>, 15 mol% HfO_2-55 mol% Y_2O_3-30 mol% Sm_2O_3; **(r)** <B>+<C>+<F>, 10 mol% HfO_2-55 mol% Y_2O_3-35 mol% Sm_2O_3; **(s)** <B>+<C>+<F>, light is <F>, gray is <C-Y_2O_3>, dark is <B-Sm_2O_3>, 10 mol% HfO_2-55 mol% Y_2O_3-35 mol% Sm_2O_3.

continued...

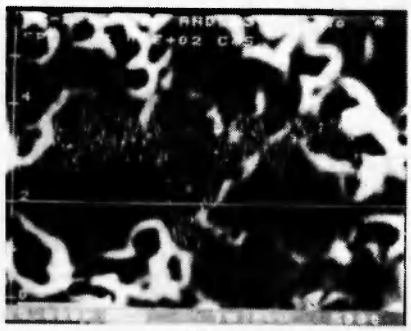
5k

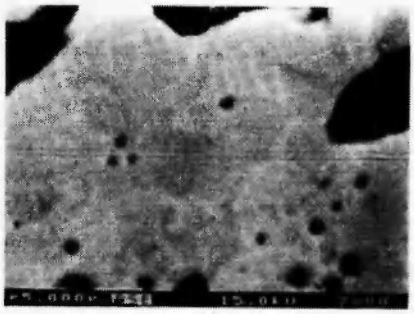
5l

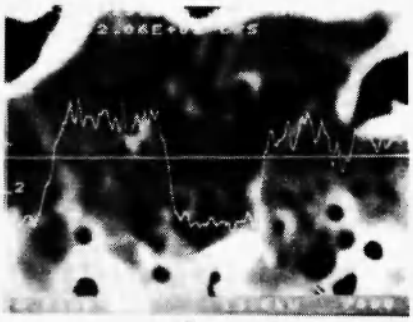
5m

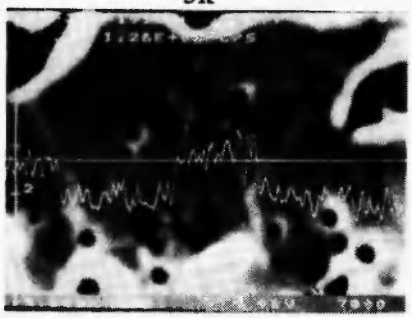
5n

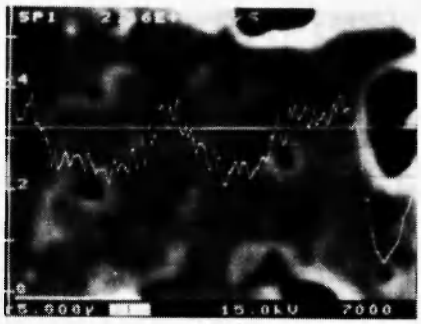
5o

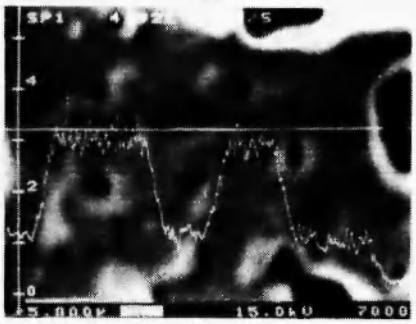
5p

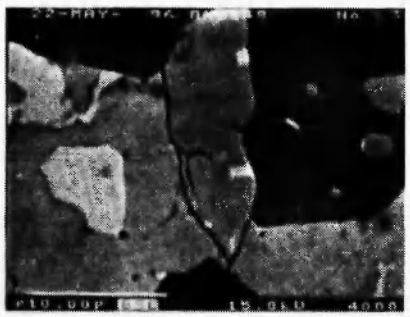
5q


5r

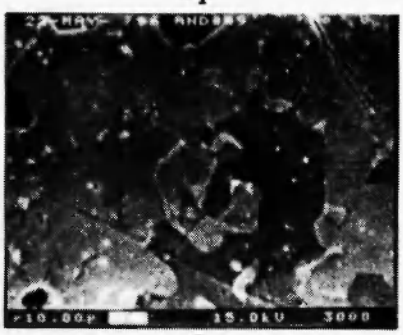
5s

microstructure of the sample is presented by light grains of 2.5-7.5 μm in size and dark intergrain phase (Fig. 5 a). From data of SEM, XRD and petrography this sample contains two phases (B+C). The local x-ray analysis was used to distinguish between the two phases. The light phase has been proved to be enriched with hafnia and yttria corresponding to solid solution based on C-Y_2O_3, and the dark one located between grains corresponds to B-Sm_2O_3 solid solution (Fig. 5 b, c). The microstructures of samples 40 mol% HfO_2-10 mol% Y_2O_3-50 mol% Sm_2O_3, 30 mol% HfO_2-35 mol% Y_2O_3-35 mol% Sm_2O_3 and 25 mol% HfO_2-37.5 mol% Y_2O_3-37.5 mol% Sm_2O_3 are two phase, and in accordance with XRD they belong to the two phase field (F+C) on the diagram. Both phases are distinctly seen in Fig. 5 d-k. The light phase is mainly represented by grains of polyhedral shape and size (length) of 3.3-10.0 μm, but the gray phase has grains of 1.3-6.0 μm in size. The distribution of the elements along the section has clearly showed that the light phase contains more hafnia while the gray phase is enriched with yttria. Therefore, the light phase is cubic solid solution of F-HfO_2, and the gray one is the solid solution based on C-Y_2O_3.

The samples responding to the three phase field (B+C+F) have identical microstructure with grain size of the light phase 1.2-6.0 μm, the gray phase 0.8-13.6 μm and the dark phase 6.8-12.0 μm (Fig. 5 l-s and Fig. 6 a, b). All these structure components (Fig. 5 q) strongly differ by contrast. Using the complex of analytical methods we concluded that the light phase was F-HfO_2

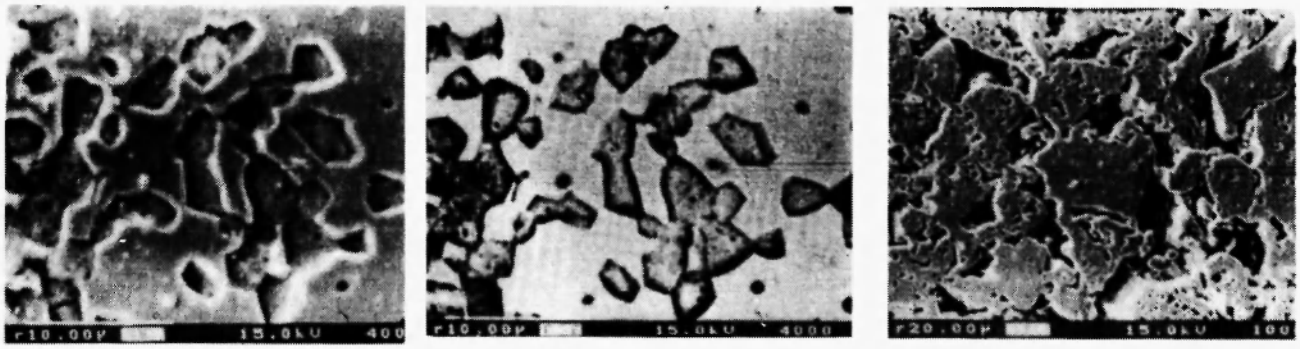

6a 6b 6c

Fig. 6. Microstructures of the samples and element distribution through the samples in the definite field of compositions of the sub-system Sm_2O_3-$Sm_2Hf_2O_7$-Y_2O_3 heat-treated at 1600 °C: **(a)** <B>+<C>+<F>, light is <F>, gray is <C-Y_2O_3>, dark is <B-Sm_2O_3>, 10 mol% HfO_2-10 mol% Y_2O_3-80 mol% Sm_2O_3; **(b)** <B>+<C>+<F>, light is <F>, gray is <C-Y_2O_3>, dark is <B-Sm_2O_3>, 10 mol% HfO_2-10 mol% Y_2O_3-80 mol% Sm_2O_3; **(c)** Py+<C>, light is <F>, gray is <C-Y_2O_3>, dark is <B-Sm_2O_3>, 45 mol% HfO_2-25 mol% Y_2O_3-30 mol% Sm_2O_3.

solid solution, the gray one was C-Y_2O_3 solid solution, and the dark phase was the solid solution based on B-Sm_2O_3.

In Fig. 6 c, the grains of two sorts are shown to be inherent in two phase field (Py+C). By the data of petrography, local x-ray analysis, the isotropic phase is the main component of smoothed grains and can be identified as solid solution based on C-Y_2O_3, while the anisotropic phase represented by porous grains is the solid solution based on samarium hafnate. The microstructures, responsible for three phase fields (Py+C+F) are shown in Figs. 7 a-c.

In the sub-system Sm_2O_3-$Sm_2Hf_2O_7$-Y_2O_3 the x-ray patterns of the following samples define the boundaries of phase fields: 45 mol% HfO_2-5 mol% Y_2O_3-50 mol% Sm_2O_3 is two phase (Py+F), 30 mol% HfO_2-55 mol% Y_2O_3-15 mol% Sm_2O_3, 25 mol% HfO_2-55 mol% Y_2O_3-20 mol% Sm_2O_3 are two phase (Py+C), 45 mol% HfO_2-10 mol% Y_2O_3-45 mol% Sm_2O_3, 45 mol% HfO_2-15 mol% Y_2O_3-40 mol% Sm_2O_3 are three phase (Py+C+F),

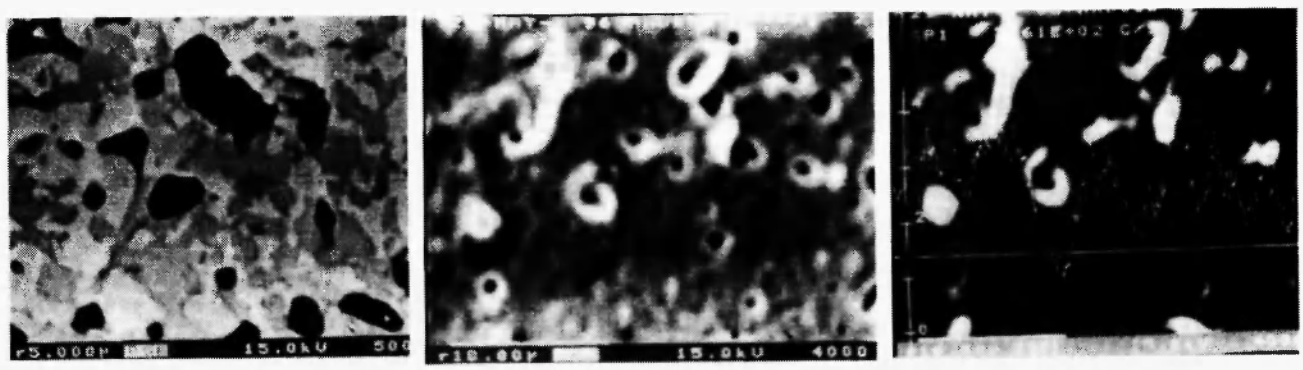

7a 7b 7c

Fig. 7. Microstructures of the samples and element distribution through the samples in the definite field of compositions of the sub-system Sm_2O_3-$Sm_2Hf_2O_7$-Y_2O_3 heat-treated at 1600 °C: **(a)** Py+<C>+<F>, matrix light - <F>, gray is Py, dark is <C>, 35 mol% HfO_2-32.5 mol% Y_2O_3-32.5 mol% Sm_2O_3; **(b)** Py+<C>+<F>, 37 mol% HfO_2-25 mol% Y_2O_3-38 mol% Sm_2O_3; **(c)** Py+<C>+<F>, Hf, 37 mol% HfO_2-25 mol% Y_2O_3-38 mol% Sm_2O_3.

40 mol% HfO_2-10 mol% Y_2O_3-50 mol% Sm_2O_3, 35 mol% HfO_2-10 mol% Y_2O_3-55 mol% Sm_2O_3 are two phase (F+C), 10 mol% HfO_2-5 mol% Y_2O_3-85 mol% Sm_2O_3 is two phase (F+B), 10 mol% HfO_2-10 mol% Y_2O_3-80 mol% Sm_2O_3, 10 mol% HfO_2-60 mol% Y_2O_3-30 mol% Sm_2O_3 are three phase (F+B+C), 5 mol% HfO_2-47.5 mol% Y_2O_3-47, 5 mol% Sm_2O_3, 3 mol% HfO_2-48.5 mol% Y_2O_3-48.5 mol% Sm_2O_3 are two phase (B+C).

CONCLUSIONS

First the phase equilibria in the system HfO_2-Y_2O_3-Sm_2O_3 at 1600 °C were studied in the whole concentration diapason. The isothermal section has been developed. No new phases were found in this ternary system. The phase fields of solid solutions based on monoclinic (B and M), cubic (C and F) polymorphous forms of rare earth oxides and hafnia, respectively, as well as pyrochlore type ordered phase of cubic symmetry $Sm_2Hf_2O_7$ (Py).

REFERENCES

1. N.Q. Minh, "Ceramic Fuel Cells,". *J. Am. Ceram. Soc.*, 76, 3, 563-588 (1993).
2. V. S. Stubican, "Recent Progress in the Field of Ceramic Systems," *Ceramics*, **36**, 5, 46-57 (1983).
3. J.Wang, H.P. Li, R. Stevens, "Review. Hafnia and hafnia-toughened ceramics", *J. Materials Science*, **27**, 12, 5397-5430 (1992).
4. F. M. Spiridonov, L. N. Komissarova, A. G. Kocharov, and V. I. Spitsin, "The System HfO_2-Y_2O_3," *J.Neorg. Chem.*, **14**, 9, 2535-2540 (1969).
5. M. Duclot, I. Vicat, and Ch. Deportes, "Mise en Evidence et Etude de la Phase Ordonnee $Y_2Hf_2O_7$ Dans le systeme HfO_2-Y_2O_3," *J. Solid State Chem.*, **2**, 4, 236-249 (1970).
6. P. Duran, "Estadio de Systeme Binarico HfO_2-Y_2O_3," *Bull. Soc. Esp. Ceram. y Vidrio*, **12**, 6, 341-346 (1973).
7. P. Duran, "Caracteristiques des Solutions Solides de Haute Temperature Entre l'Oxide de Hafnium et les Oxydes de Lanthanides," *Bull. Soc. Franc. Ceram.*, **2**, 102, 47-55 (1974).
8. D.W. Stacy and D. R. Wilder, "The Yttria-Hafnia System," *J. Am. Ceram. Soc.*, **58**, 7, 285-288 (1976).
9. A.V. Shevchenko, L. M. Lopato, and I. E. Kir'jakova, "Reactions of HfO_2 with Y_2O_3, Ho_2O_3, Er_2O_3, Tm_2O_3, Yb_2O_3 and Lu_2O_3 at High Temperatures," *Izv. Acad. Nauk SSSR, Neorg. Mater.*, **20**, 12, 1991-1996 (1984).
10. J. Lefevre, "Some Structural Modifications of Fluorite-Type Phase in the Systems Based on ZrO_2 or HfO_2," *Annual. Chim.*, **8**, 1-2, 254-256 (1963).
11. M. F. Trubelja and V. S. Stubican, "Phase Equilibria and Ordering in the System Zirconia-Hafnia-Yttria," *J. Am. Ceram. Soc.*, **71**, 8, 662-666 (1988).
12. A. V. Shevchenko, L. M. Lopato, T. V. Obolonchik, V. D. Tkachenko, and L. V. Nazarenko, "Liquidus Surface of the System HfO_2-ZrO_2-Y_2O_3," *Izv. Acad. Nauk SSSR, Neorg. Mater.*, **23**, 3, 452-456 (1987).
13. P. Duran, "The system Hafnia-Samaria", *J. Am. Ceram. Soc.*, **62**, 1-2, 9-12 (1979).
14. E.N. Isupova, V.B. Glushkova, E.K. Keler, "Study of the system HfO_2-Sm_2O_3 bellow solidus in the hafnia rich region", *Izv. Acad. Nauk SSSR, Neorg. Mater.*, **4**, 3, 399-405 (1968).
15. A. V. Shevchenko, L. M. Lopato, L. V. Nazarenko, "The systems of HfO_2 with oxides of samarium, gadolinium, terbium and dysprosium at high temperatures", *Izv. Acad. Nauk SSSR, Neorg. Mater.*, **20**, 11, 1862-1866 (1984).
16. A. V. Shevchenko, B.S. Nigmanov, Z.A. Zaitseva, L. M. Lopato, "Reactions of samaria and gadolynia with yttria", *Izv. Acad. Nauk SSSR, Neorg. Mater.*, **22**, 5, 775-778 (1986).
17. B. Hayek., E. Kalalova, H.O. Stompfova, "Tvorbe Smesnych krystalu v systemech Sm_2O_3-Y_2O_3, Sm_2O_3-Tb_2O_3 a Sm_2O_3-Dy_2O_3", *Prispevky k chemii vcachejsich prvku.*, Vys. skoly chem.-technol., Praha. B. 14, 21 (1972).